Emergent spin-1 trimerized valence bond crystal in the spin-$\frac{1}{2}$ Heisenberg model on the star lattice

Shi-Ju Ran,[1] Wei Li,[2] Shou-Shu Gong,[2,3] Andreas Weichselbaum,[4] Jan von Delft,[4] and Gang Su[5,6,*]

[1]*ICFO–Institut de Ciencies Fotoniques, The Barcelona Institute of Science and Technology, 08860 Castelldefels (Barcelona), Spain*

[2]*Department of Physics, Key Laboratory of Micro-nano Measurement-Manipulation and Physics (Ministry of Education), and International Research Institute for Multidisciplinary Science, Beihang University, Beijing 100191, China*

[3]*National High Magnetic Field Laboratory, Florida State University, Tallahassee, Florida 32310, USA*

[4]*Physics Department, Arnold Sommerfeld Center for Theoretical Physics, and Center for NanoScience, Ludwig-Maximilians-University, Munich 80333, Germany*

[5]*School of Physical Sciences and CAS Center for Excellence in Topological Quantum Computation, University of Chinese Academy of Sciences, Beijing 100049, China*

[6]*Kavli Institute for Theoretical Sciences, University of Chinese Academy of Sciences, Beijing 100190, China*

(Received 20 November 2017; revised manuscript received 15 February 2018; published 26 February 2018)

We explore the frustrated spin-$\frac{1}{2}$ Heisenberg model on the star lattice with antiferromagnetic (AF) couplings inside each triangle and ferromagnetic (FM) intertriangle couplings ($J_e < 0$), and calculate its magnetic and thermodynamic properties. We show that the FM couplings do not sabotage the magnetic disordering of the ground state due to the frustration from the AF interactions inside each triangle, but trigger a fully gapped inversion-symmetry-breaking trimerized valence bond crystal (TVBC) with emergent spin-1 degrees of freedom. We discover that with strengthening J_e, the system exhibits a universal scaling behavior either with or without a magnetic field h: the order parameter, the five critical fields that separate the J_e-h ground-state phase diagram into six phases, and the excitation gap obtained by low-temperature specific heat, all depend exponentially on J_e. Our work implies that the spin-1 VBCs can be stabilized by introducing small FM couplings in the geometrically frustrated spin-$\frac{1}{2}$ systems.

DOI: 10.1103/PhysRevB.97.075146

I. INTRODUCTION

Two-dimensional (2D) spin-$\frac{1}{2}$ frustrated magnetic systems are currently of great interest [1,2], because they may realize exotic quantum states that do not possess any semiclassical spin ordering [3], such as quantum spin liquids (QSLs) or valence bond crystals (VBCs). Leading candidates for realizing such states are spin-$\frac{1}{2}$ Heisenberg models with competing interactions on, e.g., square, honeycomb, and kagome lattices [4–20]. A particularly promising QSL system that has been argued to have experimental realizations is the kagome Heisenberg antiferromagnet (KHAF) [21–27]. However, the nature of its ground state, i.e., a gapped Z_2 spin liquid [4–8] versus a gapless U(1) Dirac spin liquid [9–13], is still under debate.

Another frustrated 2D quantum system of great potential interest is the Heisenberg model on the star lattice (Fig. 1). The star lattice is an Archimedean lattice with all sites equivalent. It is also known as the (3-12) lattice, the Fisher lattice, the decorated hexagonal or expanded kagome lattice, and the triangle-honeycomb lattice, which are well summarized in Ref. [28]. Its physics is arguably even richer than that of the KHAF, for several reasons: (a) similar to the kagome lattice, the star lattice bears a high geometrical frustration due to its triangle structure; (b) the star lattice possesses a lower coordination number than the kagome lattice, implying stronger fluctuations; (c) the star lattice naturally involves two inequivalent bonds, which can lead to exotic quantum phases; (d) various QSLs, such as the non-Abelian chiral spin liquid and the double semion spin liquid, have been found in several models on a star lattice, e.g., the Kitaev model and the quantum dimer model [28–30]; and (e) a number of organic iron acetates have been synthesized in experiments [31], which can be described by the Heisenberg model on a star lattice.

However, the Heisenberg model on a star lattice has not been fully explored yet. Recent research using the large-N approximation and a Gutzwiller projected wave function [32] only investigated the ground state for antiferromagnetic (AF) intertriangle couplings ($J_e > 0$), where a J_e-dimer VBC and a $\sqrt{3}\times\sqrt{3}$ VBC phase [33] were found (Fig. 1). However, the ground and thermal properties of the system for the ferromagnetic (FM) $J_e < 0$ are still unexplored. Recently, studying the effects of the FM couplings on 2D frustrated many-body systems has drawn a lot of interest [34,35]. One of the issues we would like to address is whether the FM couplings can adiabatically connect the spin-$\frac{1}{2}$ star model to the spin-1 kagome model [36–38].

The intrinsic importance of 2D frustrated many-body systems is matched by the great technical challenges involved in studying them. One such challenge is calculating thermodynamic properties, such as the specific heat and susceptibility. Most of the existing simulations of such systems are focused on the ground states. To compare with experiments, accurate simulations at finite temperature are strongly motivated, which are, however, scarce owing to the difficulties of such calculations [39–41].

*Corresponding author: gsu@ucas.ac.cn

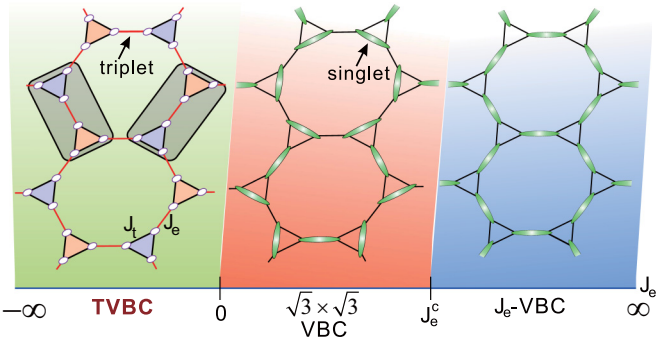

FIG. 1. The ground-state phase diagram of the star Heisenberg model. For $J_e > 0$, previous studies show various possible VBCs and spin liquids, where one recent work found a $\sqrt{3}\times\sqrt{3}$ VBC and a J_e-bond VBC [32,33]. The phase boundary J_e^c has not been settled yet. For $J_e < 0$, we show that the system is in a trimerized valence bond crystal (TVBC) phase, where a triplet appears at each J_e bond and the inversion symmetry of up and down triangles (marked by blue and yellow, respectively) is broken.

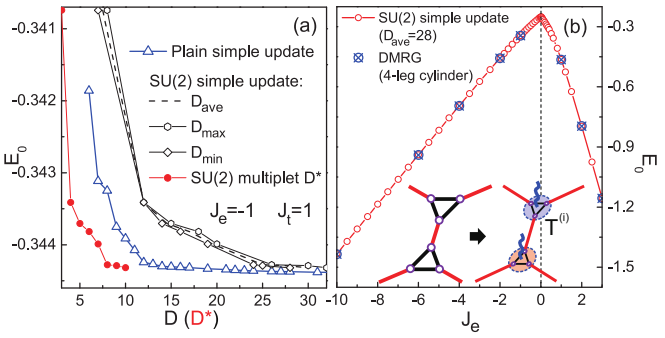

FIG. 2. (a) The ground-state energy E_0 of the star Heisenberg model for $J_e = -1$ and $J_t = 1$ obtained by the plain and SU(2) simple update algorithm, where E_0 converges versus number of states (D) and number of multiplets (D^*, red solid dots), respectively, with clearly superior performance of the SU(2)-based calculations. For comparison only, we also translate the number of multiplets D^* into the corresponding actual number of states D (black lines and symbols). Taking a fixed D^*, D of different virtual bonds may vary, according to the SU(2) fusion rules and the specific set of multiplets associated with each bond. We show the minimum, maximum, and average values of D over the three virtual bond indices of a tensor. (b) E_0 versus J_e, obtained by SU(2) simple update and DMRG simulations, which show very good agreement with each other in the whole parameter range. The inset sketches the local tensors of the TN state.

In this work, we perform a comprehensive study of the spin-$\frac{1}{2}$ Heisenberg antiferromagnet on the star lattice with FM intertriangle couplings ($J_e < 0$), calculating its ground-state and thermodynamic properties. We show that the FM intertriangle couplings do not sabotage the magnetic disordering of the ground state that arises due to frustration generated by AF intratriangle couplings, but, remarkably, trigger a trimerized valence bond crystal (TVBC) with emergent spin-1 degrees of freedom, that breaks spatial inversion symmetry. We determine the phase diagram of the system in a magnetic field and identify six phases. We uncover a magnetization cusp on the boundary between the inversion-symmetry-breaking and the non-inversion-symmetry-breaking phases. We calculate the temperature dependence of the specific heat and determine a nonmagnetic gap by analyzing accurate results for the low-temperature behavior of the specific heat. A scaling behavior versus $|J_e|$ is uncovered, evidenced by the large-J_e dependence of a range of physical quantities, such as the TVBC "order parameter," five critical fields, and the nonmagnetic gap.

II. MODEL AND METHODS

The Hamiltonian of the star Heisenberg model reads

$$H = J_e \sum_{\langle ij\rangle\in J_e} S_i \cdot S_j + J_t \sum_{\langle lm\rangle\in J_t} S_l \cdot S_m - h \sum_n \hat{S}^z. \quad (1)$$

The first summation runs over all intertriangle bonds, the second over all intratriangle bonds, and the third over all sites giving the magnetic field.

Four different state-of-the-art algorithms are employed, including the SU(2) density matrix renormalization group (DMRG) [42] on a cylindrical geometry of finite size, the simple updates with and without non-Abelian SU(2) symmetry implemented [43–45] in the thermodynamic limit, and the network contractor dynamics (NCD) [40] for the thermodynamics. These algorithms are designed for different purposes, and therefore operate differently. Overall consistency across these methods evidences a numerically unbiased, accurate, and comprehensive study.

We employ tensor network (TN) [45] and DMRG [42] methods to simulate the ground state on the infinite lattice and cylindrical geometries, respectively. To be specific, the TN representation of the ground state [inset of Fig. 2(b)] can be written as

$$|\psi\rangle = \sum_{\{s\}} \mathrm{Tr}_{\{a\}\in\mathrm{TN}} \left[\prod_j \left(T(j)^{s_{j,1}s_{j,2}s_{j,3}}_{a_{j,1}a_{j,2}a_{j,3}} |s_{j,1},s_{j,2},s_{j,3}\rangle \right) \right], \quad (2)$$

where $T(j)$ is a $(d^3\times D^3)$ tensor residing on the jth triangle with physical dimension d and ancillary bond dimension D, containing all parameters of the TN state. The ancillary bonds $\{a_{j,n}\}$ $(n = 1,2,3)$ carry the entanglement of the state and $\mathrm{Tr}_{\{a\}\in\mathrm{TN}}$ denotes a contraction of all shared $\{a_{j,n}\}$. The physical bonds $\{s_{j,n}\}$ $(n = 1,2,3)$ represent the three spins inside the jth triangle with local basis $|s_{j,n}\rangle$. Such a TN ansatz is called a projected entangled-pair state (PEPS) [43]. The simple update algorithm [45] provides an efficient way to optimize the PEPS by minimizing the energy per site $E_0 = \langle\psi|H|\psi\rangle$. The simple update has shown great efficiency and accuracy for simulating gapped systems. The observables such as magnetization can then be calculated with the PEPS.

The method for finite-temperature simulations are implemented in a similar way. Each local tensor in the TN possesses two physical bonds that correspond to the *bra* and *ket* space of the thermal state. We use the NCD approach [40] to optimize the TN. The basic idea of NCD is to approximately encode the TN contraction problem into local self-consistent eigenvalue problems that can be efficiently solved. NCD shares a similar spirit with the simple update. Their mathematical

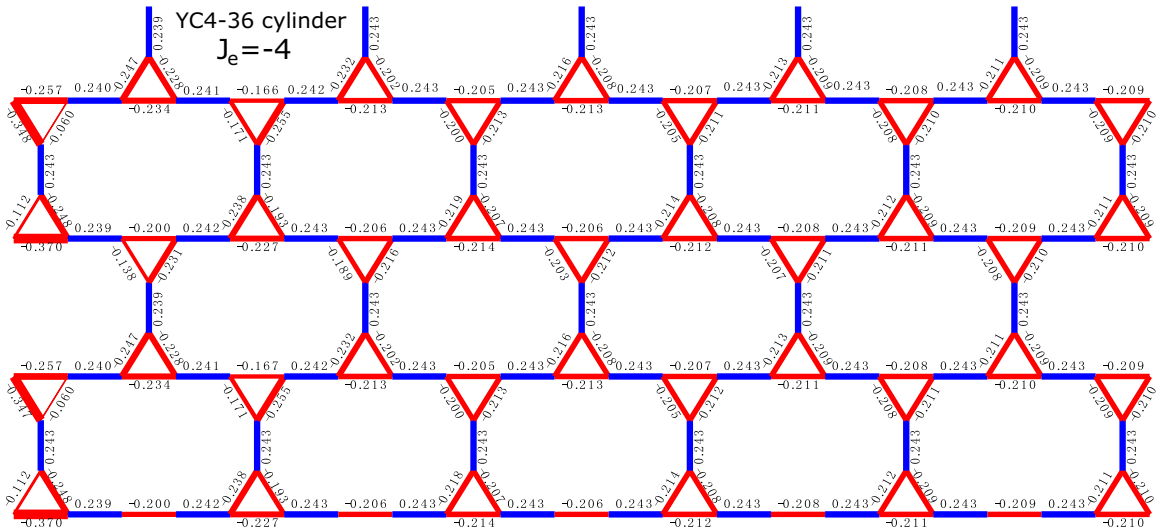

FIG. 3. The bond correlation $\langle S_i S_j \rangle$ versus distance x from the pinned boundary (using $J_{\text{pin}} = 2$) on a YC4-36 cylinder for $J_e = -4$ calculated by DMRG keeping 2000 SU(2) multiplets. The thickness indicates the strength of the bond energies.

background is the rank-1 decomposition that gives the optimal Bethe approximation of the corresponding TN [46]. The performance of such kind of approximation scheme is related to the speed of convergence to the fixed point when solving rank-1 decomposition, which is closely related to the value of gap. Thus, the algorithms show nice efficiency and accuracy for the gapped systems. The positions of the critical points that separate gapped phases can also be well determined due to the good performance within the gapped phases. At the critical points, however, it is still unclear how to optimize the tensors while keeping the criticality (such as the divergence of the correlation length) of the ansatz. Extracting critical information (e.g., critical exponents) is still a challenging task.

In addition, we implement SU(2) symmetry in TN states and related algorithms by using QSpace techniques [44]: we impose SU(2) symmetry in every single tensor index, retain the symmetry during imaginary time evolutions and other tensor manipulations, and keep track of multiplets (instead of individual states) on the bonds. We only need to optimize the reduced tensors (instead of full tensors), and thus reduce both the memory and CPU time dramatically [36,44].

We compare the ground-state energy obtained by different methods. In Fig. 2(a), we show the energy obtained by plain and SU(2) PEPS calculations, which both converge to the same results. Note that for comparable number of states D, a lower ground-state energy can be obtained by plain PEPS as compared to SU(2) PEPS, since it is allowed to break symmetries and hence has access to a larger variational parameter space. However, the results converge toward the same value for large D, suggesting that as expected, the tensors eventually converge to tensors that respect symmetries. This justifies the exploitation of symmetries at significantly reduced overall numerical cost.

In Fig. 2(b) we plot the energy obtained from SU(2) TN simulations and cylindrical DMRG for $-10.0 \leqslant J_e \leqslant 3.0$, which shows excellent agreement in the whole region. Moreover, the appearance of a cusp in the energy curve at $J_e = 0$ indicates a first-order phase transition.

III. SPONTANEOUS INVERSION SYMMETRY BREAKING

We now study the ground state of the star-lattice model, which is found to possess spontaneous inversion symmetry breaking (SISB). It can be characterized by the energy difference between the two kinds of triangles $\delta \equiv |E^{\triangle} - E^{\triangledown}|$ where we have $E^{\triangle(\triangledown)} = \langle\psi| \sum_{\langle ij\rangle \in \triangle(\triangledown)} H_{ij} |\psi\rangle$ per triangle with the summation running over all local interactions H_{ij} inside the up (down) triangles. We use DMRG to calculate the cylinder system with the geometry shown in Fig. 3 (denoted by YC4). To break the inversion symmetry between the up and down triangles, we take the couplings inside the up triangles on the open boundaries as $J_{\text{pin}} = 2J_t$ (J_t is the coupling constant for all other triangles).

Then, we measure the decaying behavior of δ from the boundary to the bulk. As shown in Fig. 4(a), we find that δ decays quite slowly for large $-J_e$, implying a large decay

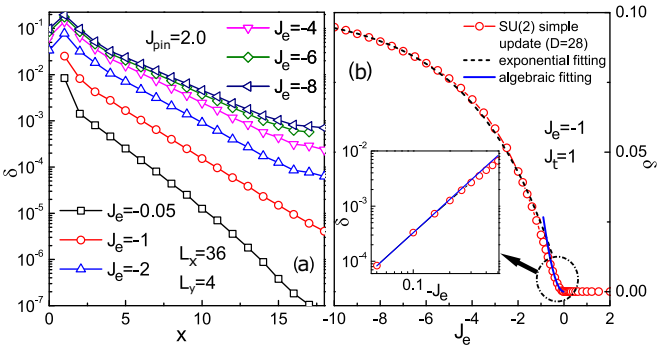

FIG. 4. (a) Log-linear plot of the inversion-symmetry-breaking parameter δ as a function of the distance x from the boundary for the YC4-36 cylinder with boundary pinning. (b) The J_e dependence of δ obtained from SU(2) simple update simulations. As long as $J_e < 0$, the system has a nonzero δ. We find by fitting that for approximately $-J_e \gg 4$, δ fulfills the relation $\delta = \tilde{\delta}(1 - e^{\mu J_e})$, where $\mu = 0.28$ and $\tilde{\delta} = 0.1$ that gives the value of δ for $J_e \to -\infty$. In contrast, for small $|J_e|$, we find $\delta = 0.03 J_e^2$ for $J_e \to 0$ (see inset).

length. We checked that different values of $J_{\rm pin}$ give the same decay length. Since the decay length for δ keeps increasing with increasing $-J_e$, our DMRG calculations imply that the SISB of the ground state might survive on a wider or even infinite-size system. Based only on the DMRG results; however, it is difficult to determine whether the symmetry breaking persists in the thermodynamic limit. With decreasing $|J_e|$, δ decays faster. For small values of $|J_e|$, the SISB is too weak to identify on a small cylinder. To provide more solid evidence, we thus employ the TN simulations on the infinite-size system.

The TN calculations, too, find a strong TVBC order for large $|J_e|$ [Fig. 4(b)], consistent with DMRG results. By fitting the order parameter δ with $-J_e \gg 0$, we find that δ fulfills an exponential behavior with J_e as

$$\delta = \tilde{\delta}(1 - e^{\mu J_e}), \tag{3}$$

where we have $\mu = 0.28$ and $\tilde{\delta} = 0.1$. It indicates that the large $|J_e|$ couplings project each corresponding spin-$\frac{1}{2}$ pair into an effective $S = 1$ spin, and stabilize a TVBC. Interestingly, for the small $|J_e|$ region, the TN simulations show that the inversion symmetry is broken for any small $J_e < 0$, while such a symmetry is found to be intact for $J_e > 0$. To be specific, for $-J_e \to 0$, δ satisfies the algebraic relation $\delta = 0.03 J_e^2$, as shown in the inset of Fig. 4(b). Our results not only support the TVBC ground state for the spin-1 kagome model [36–38], but also further show that such a TVBC is robust in the spin-$\frac{1}{2}$ star model for any finite strength of the FM J_e interactions. In other words, the TVBC survives with the fluctuations caused by the finiteness of J_e. In contrast to the spin-1 model, two spin-$\frac{1}{2}$'s in our system are not strictly projected into the spin-1's, especially for small $|J_e|$.

Note that in the $J_e \to -\infty$ limit, each two spin-$\frac{1}{2}$'s connected by a ferromagnetic coupling are strictly mapped to the triplet states, i.e., a spin-1. Each antiferromagnetic coupling between two spin-$\frac{1}{2}$'s is then exactly mapped to the antiferromagnetic coupling of two spin-1's. The Hamiltonian of our star model becomes identical to that of the spin-1 antiferromagnetic Heisenberg model on the kagome lattice.

IV. GROUND-STATE PHASE DIAGRAM IN MAGNETIC FIELDS

In a magnetic field, frustrated magnetic systems usually exhibit distinct features in the magnetization curve such as cusps [47] and plateaus [48], which reveal the exotic structure of the energy spectrum and distinguish different phases. We study the field dependence of the ground-state magnetization per site $M_z = \sum_n \langle\psi|\hat{S}_n^z|\psi\rangle/N$ and the energy difference δ, as shown in Fig. 5. Interestingly, we find a zero plateau corresponding to a finite spin gap, a cusp representing the restoration of inversion symmetry, and a $\frac{1}{3}$ plateau in the magnetization curve.

In the zero plateau region, $h < h_{c1}$, both M_z and δ remain unchanged, indicating that there is a finite spin gap protecting the TVBC state. With increasing h, the spin gap decreases and eventually closes at $h = h_{c1}$. For $h > h_{c1}$, M_z becomes nonzero and δ starts to decrease. At $h = h_{c2}$, a cusp appears in M_z and δ vanishes, separating the SISB phase from the $M_z \neq 0$ normal phases. A magnetization cusp has also been observed in some one-dimensional frustrated magnetic systems having

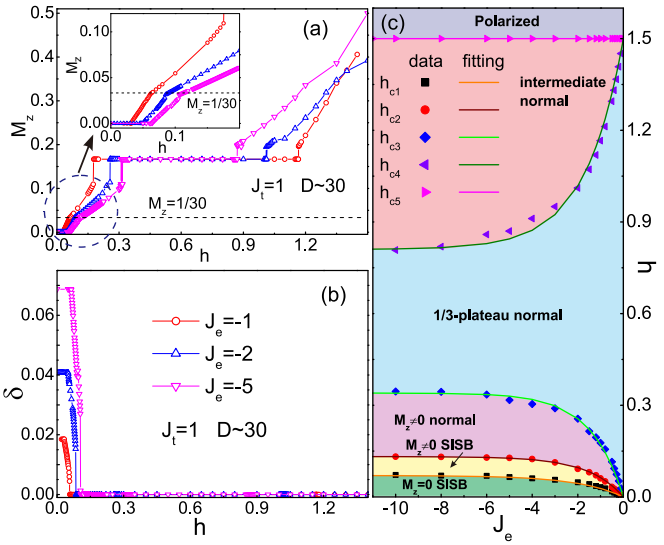

FIG. 5. The field dependence of (a) the magnetization M_z and (b) the TVBC order parameter δ. Five critical fields h_{ci} ($i = 1,2,\ldots,5$) is determined by M_z and δ, which determine six phases in the J_e-h diagram as shown in (c). For $0 \leqslant h < h_{c1}$, $M_z = 0$ and δ is intact. For $h_{c1} < h < h_{c2}$, M_z increases, and δ starts to diminish and vanishes at $h = h_{c2}$, where the inversion symmetric and symmetry-breaking phases are separated and one always has $M_z = 1/30$. For $h_{c3} < h < h_{c4}$, the system is in a conventional $\frac{1}{3}$-plateau solid phase. Here, we use the simple update algorithm of PEPS with $D \sim 30$.

ground states that break lattice symmetry, reflecting the novel energy dispersion of the low-lying excitations [47]. A first shoulder in the magnetization occurs consistently around $M \simeq 1/30$. By further increasing the field, we find a $\frac{1}{3}$ plateau corresponding to a gapped solid state [48]. Based on the behaviors of M_z and δ we obtain the quantum phase diagram in the J_e-h plane, shown in Fig. 5(c).

We find that the critical fields h_{ci} ($i = 1,2,\ldots,5$) also converge exponentially for large $|J_e|$,

$$h_{ci} = \tilde{h}_{ci}(1 - \alpha_i e^{\nu_i J_e}), \tag{4}$$

as shown in Fig. 5(c), with coefficients given in Table I. The scaling behavior of the critical fields strongly implies that the star Heisenberg model approaches the effective spin-1 model in an exponential manner, suggesting that the large $|J_e|$ represents a gapped system, consistent with the existing works [36–38].

TABLE I. Values for the fitting parameters $\tilde{h}_{ci}$, α_i, and ν_i of the critical fields [see Eq. (4)]. Note that as $h_{c5} = 1.5$ is a constant, we have $\alpha_5 = 0$ and any ν_5.

	h_{c1}	h_{c2}	h_{c3}	h_{c4}	h_{c5}
$\tilde{h}_{ci}$	0.07	0.132	0.34	0.81	1.5
α_i	1	1	1	−0.85	0
ν_i	0.5	0.65	0.7	0.6	*

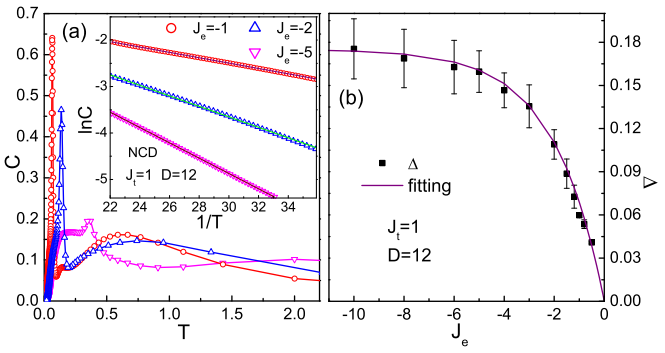

FIG. 6. (a) The temperature dependence of specific heat C for various J_e, where multipeak structures are observed. We use the NCD algorithm with $D = 12$. The position of the low-temperature peak moves to the higher temperature as $-J_e$ increases. Inset: the curve of $\ln C$ versus inverse temperature $1/T$. Below the low-temperature peak, one can see that the specific heat decays exponentially with $1/T$ as $\ln C = -\Delta/T + \text{const}$, where Δ is the (J_e-dependent) excitation gap. (b) By fitting specific heat, the excitation gap Δ for different J_e is obtained and shown to fulfill the relation $\Delta = \tilde{\Delta}(1 - e^{\kappa J_e})$. The error bars are given by the linearity of $\ln C$ at the low temperatures [50]. By fitting the $\Delta - J_e$ curve, we have $\tilde{\Delta} = 0.175$ that gives the excitation gap in the $J_e \to -\infty$ limit and the constant $\kappa = 0.5$.

V. SPECIFIC HEAT

The calculation of specific heat is important for comparing with the experiments, where it can be directly measured by mature techniques, e.g., a thermal relaxation calorimeter. Thermal properties reflect not only the ground state, but also different physics at different temperature/energy scales.

In Fig. 6(a), we plot the calculated specific heat curves for various J_e. Changing J_e from zero to $-\infty$, we observe that the low-temperature peak of the specific heat C moves to higher temperature and merges with other peaks. From the inset, one can see that below the low-temperature peak, $\ln C$ depends linearly on the inverse temperature $1/T$ as $\ln C = -\Delta/T + \text{const}$, indicating a finite gap Δ that is consistent with the gapped TVBC ground state. The J_e dependence of Δ is given in Fig. 6(b). We observe again the exponential scaling behavior on Δ as

$$\Delta = \tilde{\Delta}(1 - e^{\kappa J_e}), \tag{5}$$

where a fit yields $\kappa = 0.5$ and $\tilde{\Delta} = 0.17 \pm 0.02$ corresponding to the gap for $J_e \to -\infty$. Incidentally, simulations on the spin-1 kagome model also show a spin singlet gap $\tilde{\Delta} = 0.1$–0.2 [49].

In principle, Δ is obtained from the low-temperature C, and should give the gap of the lowest excitation. In the given context, we expect $\Delta \sim h_{c1}$. Comparing with the critical fields, however, we find $\Delta \sim h_{c2}$, which should give the gap protecting spatial inversion symmetry of the up and down triangles. We provide the following scenario to explain our observations. The gaps for the excitations with $S \geqslant 1$ normally satisfy a linear relation as $\Delta(S) \sim S$, which leads to a nonzero magnetization when h becomes larger than the spin gap. However, this linear relation may not be always true. Exceptions have been found when the system has ferromagnetic interactions [51]. This means it is possible that nonzero magnetization appears at the h smaller than the spin gap. In our model at $h = 0$, the lowest excitation is the $S = 1$ triplet state with the spin gap $\Delta \sim h_{c2}$ (this gap also protects the spatial inversion symmetry). Then nonzero magnetization appears with $h < h_{c2}$, say at h_{c1} in our case, and the first excitation gap should be h_{c2} at $h = 0$.

On the other hand, we cannot completely exclude another possibility, where $\Delta \sim h_{c2}$ may be just a coincidence, caused by the computational error. We are unable to give a conclusive answer here due to the lack precision of the existing methods. Developing new approaches with higher accuracy for 2D models especially at the low temperatures would be necessary. But in any case, we would like to stress that this issue causes no harm to our main achievement, which is the TVBC with an exponential scaling behavior.

VI. CONCLUSIONS

In this work, we discover an emergent spin-1 TVBC with spontaneous lattice inversion symmetry breaking in the spin-$\frac{1}{2}$ star Heisenberg model with FM intertriangle couplings, and study its ground-state and thermodynamic properties. We employ four different algorithms including SU(2) DMRG, simple update of the TN state with and without SU(2) symmetry, and NCD. Rich properties that define the exotic TVBC phase are revealed, including fruitful phases in a magnetic field, the magnetic cusps at $M_z \simeq 1/30$, and the universal exponential scaling behavior. Our work implies that spin-1 VBCs can be stabilized in the geometrically frustrated spin-$\frac{1}{2}$ star-lattice systems with an arbitrary strength of the FM interactions. Moreover, our calculations of the specific heat provide useful data at finite temperatures which can be compared directly with the future experiments.

ACKNOWLEDGMENTS

We are indebted to C. Peng for useful discussions. This work was supported in part by the MOST of China (Grants No. 2012CB932900 and No. 2013CB933401), the Strategic Priority Research Program of the Chinese Academy of Sciences (Grant No. XDB07010100), and NSFC Grant No. 11474249. S.S.G. was supported by the National Science Foundation through Grant No. DMR-1408560, and the National High Magnetic Field Laboratory that is supported by NSF DMR-1157490 and the State of Florida. W.L. was supported by SFB-TR12 and the National Natural Science Foundation of China (Grant No. 11504014), and A.W. by DFG WE4819/1-1 and WE4819/1-2. S.J.R. was supported by ERC AdG OSYRIS (ERC-2013-AdG Grant No. 339106), the Spanish MINECO grants FOQUS (Grant No. FIS2013-46768-P), FISICATEAMO (Grant No. FIS2016-79508-P), and "Severo Ochoa" Programme (SEV-2015-0522), Catalan AGAUR SGR 874, Fundació Cellex, EU FETPRO QUIC, EQuaM (FP7/2007-2013 Grant No. 323714), and CERCA Programme/Generalitat de Catalunya, and Fundació Catalunya-La Pedrera · Ignacio Cirac Program Chair.

[1] L. Balents, Nature (London) **464**, 199 (2010).

[2] J. Richter, J. Schulenburg, and A. Honecker, Lect. Notes Phys. **645**, 85 (2004).

[3] H. T. Diep, *Frustrated Spin Systems* (World Scientific, Singapore, 2004).

[4] S. Yan, D. Huse, and S. R. White, Science **332**, 1173 (2011).

[5] S. Depenbrock, I. P. McCulloch, and U. Schollwöck, Phys. Rev. Lett. **109**, 067201 (2012).

[6] H. C. Jiang, Z. H. Wang, and L. Balents, Nat. Phys. **8**, 902 (2012).

[7] S. Nishimoto, N. Shibata, and C. Hotta, Nat. Commun. **4**, 2287 (2013).

[8] J. W. Mei, J. Y. Chen, H. He, and X. G. Wen, Phys. Rev. B **95**, 235107 (2017).

[9] Y. Ran, M. Hermele, P. A. Lee, and X. G. Wen, Phys. Rev. Lett. **98**, 117205 (2007).

[10] M. Hermele, Y. Ran, P. A. Lee, and X.-G. Wen, Phys. Rev. B **77**, 224413 (2008).

[11] Y. Iqbal, F. Becca, S. Sorella, and D. Poilblanc, Phys. Rev. B **87**, 060405(R) (2013).

[12] Y. Iqbal, D. Poilblanc, and F. Becca, Phys. Rev. B **89**, 020407(R) (2014).

[13] Y. C. He, M. P. Zaletel, M. Oshikawa, and F. Pollmann, Phys. Rev. X **7**, 031020 (2017).

[14] Y. C. He, D. N. Sheng, and Y. Chen, Phys. Rev. Lett. **112**, 137202 (2014).

[15] S. S. Gong, W. Zhu, and D. N. Sheng, Sci. Rep. **4**, 6317 (2014).

[16] B. Bauer, L. Cincio, B. P. Keller, M. Dolfi, G. Vidal, S. Trebst, and A. W. W. Ludwig, Nat. Commun. **5**, 5137 (2014).

[17] R. Ganesh, J. van den Brink, and S. Nishimoto, Phys. Rev. Lett. **110**, 127203 (2013).

[18] Z. Y. Zhu, D. A. Huse, and S. R. White, Phys. Rev. Lett. **110**, 127205 (2013).

[19] S. S. Gong, D. N. Sheng, O. I. Motrunich, and M. P. A. Fisher, Phys. Rev. B **88**, 165138 (2013).

[20] S. S. Gong, W. Zhu, D. N. Sheng, O. I. Motrunich, and M. P. A. Fisher, Phys. Rev. Lett. **113**, 027201 (2014).

[21] P. Mendels, F. Bert, M. A. de Vries, A. Olariu, A. Harrison, F. Duc, J. C. Trombe, J. S. Lord, A. Amato, and C. Baines, Phys. Rev. Lett. **98**, 077204 (2007).

[22] J. S. Helton, K. Matan, M. P. Shores, E. A. Nytko, B. M. Bartlett, Y. Yoshida, Y. Takano, A. Suslov, Y. Qiu, J.-H. Chung, D. G. Nocera, and Y. S. Lee, Phys. Rev. Lett. **98**, 107204 (2007).

[23] M. A. de Vries, J. R. Stewart, P. P. Deen, J. Piatek, G. N. Nilsen, H. M. Ronnow, and A. Harrison, Phys. Rev. Lett. **103**, 237201 (2009).

[24] D. Wulferding, P. Lemmens, P. Scheib, J. Röder, P. Mendels, S. Chu, T. Han, and Y. S. Lee, Phys. Rev. B **82**, 144412 (2010).

[25] B. Fåk, E. Kermarrec, L. Messio, B. Bernu, C. Lhuillier, F. Bert, P. Mendels, B. Koteswararao, F. Bouquet, J. Ollivier, A. D. Hillier, A. Amato, R. H. Colman, and A. S. Wills, Phys. Rev. Lett. **109**, 037208 (2012).

[26] T. H. Han, J. S. Helton, S. Chu, D. G. Nocera, J. A. Rodriguez-Rivera, C. Broholm, and Y. S. Lee, Nature (London) **492**, 406 (2012).

[27] L. Clark, J. C. Orain, F. Bert, M. A. De Vries, F. H. Aidoudi, R. E. Morris, P. Lightfoot, J. S. Lord, M. T. F. Telling, P. Bonville, J. P. Attfield, P. Mendels, and A. Harrison, Phys. Rev. Lett. **110**, 207208 (2013).

[28] J. O. Fjaerestad, arXiv:0811.3789.

[29] H. Yao and S. A. Kivelson, Phys. Rev. Lett. **108**, 247206 (2012).

[30] Y. Qi, Z. C. Gu, and H. Yao, Phys. Rev. B **92**, 155105 (2015).

[31] Y. Z. Zheng, M. L. Tong, W. Xue, W. X. Zhang, X. M. Chen, F. Grandjean, and G. J. Long, Angew. Chem., Int. Ed. **46**, 6076 (2007).

[32] B. J. Yang, A. Paramekanti, and Y. B. Kim, Phys. Rev. B **81**, 134418 (2010).

[33] Note that some former research by several methods also indicated other possible VBCs and QSLs. See, e.g., J. Richter, J. Schulenburg, A. Honecker, and D. Schmalfuß, Phys. Rev. B **70**, 174454 (2004); G. Misguich and P. Sindzingre, J. Phys.: Condens. Matter **19**, 145202 (2007); T. P. Choy and Y. B. Kim, Phys. Rev. B **80**, 064404 (2009).

[34] S. Bieri, L. Messio, B. Bernu, and C. Lhuillier, Phys. Rev. B **92**, 060407(R) (2015).

[35] D. Boldrin, B. Fåk, M. Enderle, S. Bieri, J. Ollivier, S. Rols, P. Manuel, and A. S. Wills, Phys. Rev. B **91**, 220408(R) (2015).

[36] T. Liu, W. Li, A. Weichselbaum, J. von Delft, and G. Su, Phys. Rev. B **91**, 060403(R) (2015).

[37] H. J. Changlani and A. M. Läuchli, Phys. Rev. B **91**, 100407(R) (2015).

[38] T. Picot and D. Poilblanc, Phys. Rev. B **91**, 064415 (2015).

[39] S. J. Ran, W. Li, B. Xi, Z. Zhang, and G. Su, Phys. Rev. B **86**, 134429 (2012).

[40] S. J. Ran, B. Xi, T. Liu, and G. Su, Phys. Rev. B **88**, 064407 (2013).

[41] P. Czarnik, L. Cincio, and J. Dziarmaga, Phys. Rev. B **86**, 245101 (2012); P. Czarnik and J. Dziarmaga, *ibid.* **90**, 035144 (2014); **92**, 035120 (2015).

[42] S. R. White, Phys. Rev. Lett. **69**, 2863 (1992); Phys. Rev. B **48**, 10345 (1993).

[43] F. Verstraete and J. I. Cirac, arXiv:cond-mat/0407066; J. Jordan, R. Orús, G. Vidal, F. Verstraete, and J. I. Cirac, Phys. Rev. Lett. **101**, 250602 (2008).

[44] A. Weichselbaum, Ann. Phys. (NY) **327**, 2972 (2012).

[45] H. C. Jiang, Z. Y. Weng, and T. Xiang, Phys. Rev. Lett. **101**, 090603 (2008); Z. Y. Xie, H. C. Jiang, Q. N. Chen, Z. Y. Weng, and T. Xiang, *ibid.* **103**, 160601 (2009).

[46] S. J. Ran, E. Tirrito, C. Peng, X. Chen, G. Su, and M. Lewenstein, arXiv:1708.09213.

[47] K. Okunishi, Y. Hieida, and Y. Akutsu, Phys. Rev. B **60**, R6953(R) (1999).

[48] M. Oshikawa, M. Yamanaka, and I. Affleck, Phys. Rev. Lett. **78**, 1984 (1997).

[49] H. J. Changlani and A. M. Läuchli (private communication).

[50] Note that the error bars only indicate the error from fitting. The total error should also include the error inherent to the choice of the algorithm and, due to finite numerical resources, the Trotter-Suzuki error, and the accumulated truncation error. There is no known method to estimate their combined effect on the total error.

[51] N. Shannon, T. Momoi, and P. Sindzingre, Phys. Rev. Lett. **96**, 027213 (2006).